THE JOURNAL OF PHYSICAL CHEMISTRY C
A JOURNAL OF THE AMERICAN CHEMICAL SOCIETY

pubs.acs.org/JPCC

Article

Defect Pairs in Boron Nitrides That Exhibit Strong Electronic Transitions in the Infrared

Seungyeop Lee, Jacob Fortner, and YuHuang Wang*

Cite This: J. Phys. Chem. C 2024, 128, 11672−11678

Read Online

ACCESS | Metrics & More | Article Recommendations | Supporting Information

ABSTRACT: Vacancy and substitution defects in boron nitrides display quantum emission properties promising for various technological applications in biosensing, imaging, telecommunications, and quantum optical computing. However, such atomic defects and their associated properties have thus far been limited to the ultraviolet and visible spectral range. In this work, we explored sp^3-hybridized defect pairs in boron nitrides using density functional theory and found that optically active defect transitions can occur in the infrared with a high oscillator strength that is 6.5 times as high as that of boron nitride's band gap transition. This phenomenon was observed in nanotubular and hexagonal boron nitrides, suggesting that these IR properties of sp^3 defects can generally be found in boron nitrides.

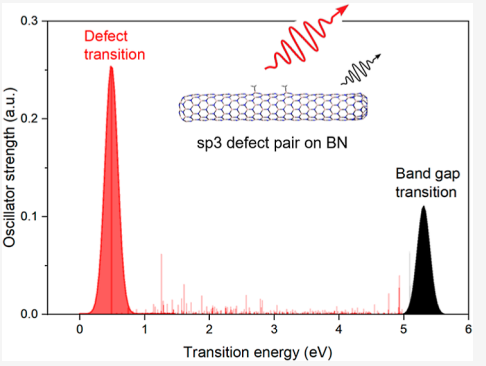

INTRODUCTION

Boron nitrides (BNs), a family of sp^2-hybridized boron and nitrogen atoms exemplified by boron nitride nanotubes (BNNTs) and hexagonal boron nitride (h-BN), feature a strong in-plane polar bond that endows the nanostructure with excellent mechanical properties and high thermal resistivity, in addition to being an electrical insulator (band gap ∼5.9 eV).[1−6] BNs are also biocompatible,[7,8] suggesting their potential in biomedical applications, particularly as biosensors.[2,9] However, the optical transitions of BNs occur in the ultraviolet (UV) spectral range, which prevents their applications in the near-infrared (IR) biological tissue transparency windows.[10,11] Similarly, the UV emission of BNs limits their application for telecommunications in optical fibers and free space between satellites, as well as photonic qubits for quantum computing where IR emitters are needed.[12−14]

The optical properties of crystalline materials can be modified by incorporating atomic defects into the lattice structure, as observed in diamond,[15,16] tungsten-diselenide,[17] single-walled carbon nanotubes,[18,19] and h-BN.[20,21] Such defects can exhibit single-photon emission, making them promising for various quantum technology applications.[15−17,22−29] In particular, sp^3 defects in semiconducting carbon nanotube hosts have emerged as a family of quantum emitters with versatile functionality. Through covalent functionalization of the sp^2-hybridized lattice, quantum defect states are created within the carbon nanotube band gap, leading to optically active electronic transitions that significantly red shift from the band gap emission. As a result, new emission peaks can be produced that are tunable in the near-IR, including telecom wavelengths and in the tissue transparent NIR-II window, by chemically and physically tailoring the defect functional groups.[18,19,30−37]

While there have been studies on the electronic structures of vacancy and substitution defects in BNs (with the defect emission ranging from 1.65 to 4.4 eV),[38−40] the effects of sp^3 defects are largely unexplored. BNs feature a similar sp^2-hybridized lattice as graphene and carbon nanotubes; however, the polar nature of the nitrogen−boron bonds (compared to nonpolar carbon−carbon bonds) may impact the electronic structure of sp^3 defects differently. Furthermore, in contrast with semiconducting carbon nanotubes, BNs are insulators, which could also impact the electronic structure of sp^3 defects. Recently, Shiraki et al. found that introducing sp^3 defects in BNNTs with hexyl functional groups on boron sites results in defect-induced photoluminescence at ∼3.7 eV (334 nm).[41] However, this defect emission lies in the UV range, making it unsuitable for imaging and sensing applications in the IR. A greater understanding of the electronic structure of sp^3 defects in BNNTs, and BNs in general, is needed to better control the optical properties of atomic defects in BNs.

In this study, we explored sp^3 quantum defects in BNs as potential bright and tunable sources of quantum emission using density functional theory (DFT) and time-dependent

Received: March 11, 2024
Revised: June 19, 2024
Accepted: July 2, 2024
Published: July 9, 2024

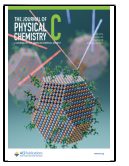

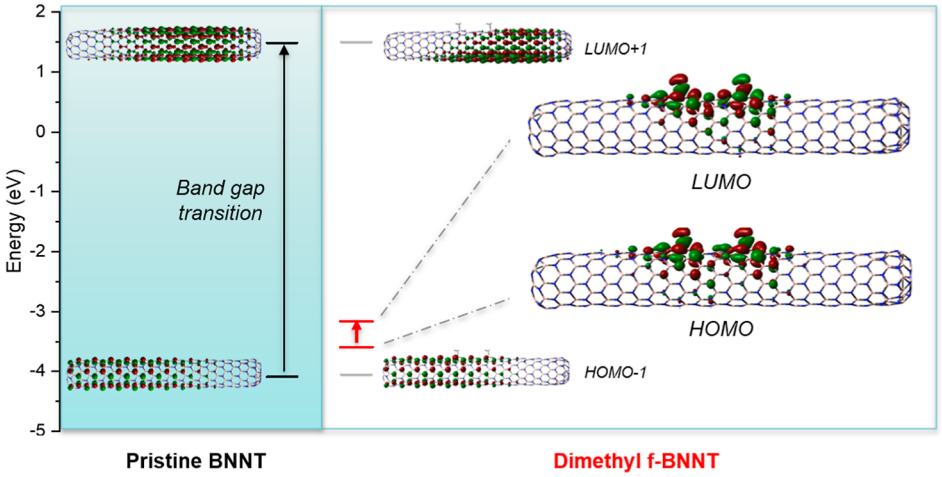

Figure 1. Defect states generated within the band gap of a BNNT by covalently bonding a pair of methyl groups to two boron atoms ~0.9 nm apart. The energy levels and frontier orbitals (isovalue = 0.01) are plotted for the pristine BNNT (left) and boron-site dimethyl functionalized f-BNNT (right). The black and red lines represent the HOMO and LUMO energy states of the pristine and f-BNNT, respectively. Gray lines represent the band edge states for the f-BNNT (HOMO − 1 and LUMO + 1). The calculated band gap for the pristine BNNT is 5.6 eV, and the HOMO−LUMO energy gap for the f-BNNT is 0.43 eV. The paired sp^3 defects enhance the frontier orbital overlap in the f-BNNT. Electron density is represented by the red (positive phase) and green (negative phase) lobes of the molecular orbitals.

DFT (TD-DFT) calculations. We found that the incorporation of methyl group pairs at both boron and nitrogen sites in BNNTs generates defect energy states within the band gap. The oscillator strength, which characterizes the likelihood of electromagnetic radiation associated with an electron transition, and the energy of these sp^3 defect transitions in BNNTs were analyzed and compared with pristine BNNTs. The electronic transitions between defect states were found to be optically allowed and red-shifted to the IR compared with the UV range band gap transition. Furthermore, we show that the sp^3 defect transition can be tuned from 0.21 to 0.63 eV (1967−5900 nm) by varying the distance between the two methyl groups. The oscillator strength of these sp^3 defects is 6.5 times as high as that of the band gap transition of the pristine BNNT and 1.5 times higher than the brightest vacancy and substitution defects in BNNTs. Additionally, we calculated the defect energy states of sp^3-functionalized h-BN and found that the defect energy gap (0.439 eV) is similar to the defect transition energy of a sp^3-functionalized (9,0)-BNNT (0.447 eV) of the same supercell size, highlighting that the defect interactions in h-BN behave similarly as that in BNNTs. These findings suggest the potential of BNs as bright and chemically tunable IR light sources through controlled manipulation of the sp^3 defect pair spacing with potential for telecommunications, quantum computing, and biosensing.[9,12−14]

METHODOLOGY AND COMPUTATIONAL DETAILS

To form sp^3 defects, we investigated methyl group pairs covalently functionalized on either boron or nitrogen sites in BNNTs.[32] Due to the large band gap of BNNTs, there is little chirality dependence on their electronic structure.[2] Therefore, we chose a 5 nm-long (9,0) BNNT as a representative model. The zigzag structure of the (9,0) chirality also allowed us to preserve the mirror symmetry along the BNNT axis such that the angular displacements of the two methyl functional groups could be neglected. The BNNT model coordinates were built using a nanotube modeler (JCrystalSoft, 2018), and defects were edited with GaussView (version 6.0.16) and Avogadro (version 1.2).[42,43] To reduce edge effects, both ends of the BNNT were capped with hemispheres of BN fullerene.[44] To introduce a pair of methyl sp^3 defects, we added CH_3 functional groups on either both boron sites or both nitrogen sites along the nanotube axis. The distances between the two methyl groups were 0.45, 0.9, 1.35, and 1.8 nm, equivalent to the distance of 1−4 unit cells in a (9,0)-BNNT. To assess the impact of the long-range interaction, we also performed TD-DFT calculations for a pristine BNNT and 0.45 and 1.8 nm spaced f-BNNT at the CAM-B3LYP/3-21G and wB97XD/3-21G level of theory.

To predict the spectral features of the f-BNNT, we first conducted DFT calculations to optimize the ground-state geometry and then computed the energy states near the band edge. TD-DFT calculations were then conducted on the optimized ground-state geometry to evaluate the oscillator strength associated with each allowed transition. As a control, DFT and TD-DFT calculations for pristine BNNTs were also conducted. Finally, we compared the oscillator strength of the sp^3 defects with that of vacancy and substitution defects (V_NN_B, V_NC_B, V_N, and V_B). All DFT calculations were conducted with Gaussian09 and Gaussian16 software packages and visualized using GaussView. Geometry optimization and TD-DFT calculations were conducted for all models at the B3LYP/STO-3G level of theory, which gave consistent results with a larger basis set (B3LYP/3-21G) for control models.

An infinite h-BN sheet was modeled using two-dimensional periodic boundary conditions (PBCs) with a periodic cell size of ~2.5 × 2.5 nm. For a more direct comparison between the h-BN and BNNT, an infinitely long BNNT was modeled using a one-dimensional PBC with a periodic cell size of ~2.5 nm. The h-BN and BNNT supercells used contained 216 atoms (or 224 with the addition of the two CH_3 defects). Models with defects were produced by attaching the methyl groups to two boron atoms 0.9 nm apart. All PBC models were geometry optimized using the B3LYP/STO-3G level of theory as implemented in Gaussian 09.

https://doi.org/10.1021/acs.jpcc.4c01586
J. Phys. Chem. C 2024, 128, 11672−11678

RESULTS AND DISCUSSION

We utilized DFT to model two methyl groups covalently bound to boron sites of a 5 nm-long pristine (9,0)-BNNT to form a pair of sp^3 defects on the nanotube (f-BNNT; see Methods for details). Defect pairs, rather than individual defects, were studied here to ensure that there was no free radical in the BNNT structure.[32] We initially set the distance between the dimethyl groups at ∼0.9 nm, equivalent to the length of 2 unit cells. Figure 1 shows the calculated frontier orbitals of the f-BNNT in comparison with the pristine BNNT control. The presence of the methyl group pair causes two defect states to form within the band gap, resulting in a new highest occupied molecular orbital (HOMO) to lowest unoccupied molecular orbital (LUMO) transition with an energy of 0.43 eV, which is significantly lower than the BN band gap transition (5.6 eV), as shown in Figure 1.

We then used TD-DFT to calculate the oscillator strength of the band gap transitions of the pristine BNNT and defect transitions of the dimethyl f-BNNT to determine the likelihood of photon absorption or emission. As shown in Figure 2a, only a low (0.039 in oscillator strength) photon absorption is expected for the pristine band gap transition. However, after the introduction of the two methyl groups to the BNNT, we observed the formation of many defect transitions within the band gap (Figure 2b, red vertical lines), the lowest energy of which features a strong oscillator strength that occurs at 0.4 eV (Figure 2b, red curve), which is significantly red-shifted from the band gap transition energy (Figure 2b, black curve). The oscillator strength of this main defect transition is 0.253, which is ∼6.5 times larger than that of the pristine band gap transition.

This high oscillator strength of the defect transition can be attributed to the strong orbital overlap between the HOMO and LUMO states in the f-BNNT. Compared with the pristine BNNTs, where the HOMO and LUMO are localized at the nitrogen and boron sites, respectively, for the f-BNNT, the HOMO and LUMO are both strongly localized around the sp^3 defect sites, as shown in Figure 1. This localization of electrons results in a good spatial overlap between the HOMO and LUMO, which causes the transition dipole moment to increase.[45] Since oscillator strength is proportional to the transition dipole moment squared, the enhanced orbital overlap between the two defect states contributes to the high oscillator strength.[46]

In addition to the defect transition having a high oscillator strength, the oscillator strength of the band gap transition of the f-BNNT is also increased ∼twofold compared to the pristine BNNT (Figure 2, black curves). This may be due to the sp^3 defects that weakly localize the electrons around the defect sites in the HOMO − 1 and LUMO + 1 states (Figure 1). Localization of electrons in both HOMO − 1 and LUMO + 1 causes stronger overlap of the band gap transition orbitals compared with those in the pristine BNNT, which in turn increases the oscillator strength of the band gap transition of the f-BNNT. Additionally, the band gap transition energy of the pristine BNNT at the highest oscillator strength is 5.36 eV, and that of the f-BNNT is 5.30 eV. We hypothesize that this 60 meV red shift occurs due to the symmetry breaking that takes place when sp^3 defects are incorporated, forming a slight dipole moment along the B−C bond (B from BNNT and C from the methyl defect functional group). This was also previously predicted in the carbon nanotube system, in which calculations

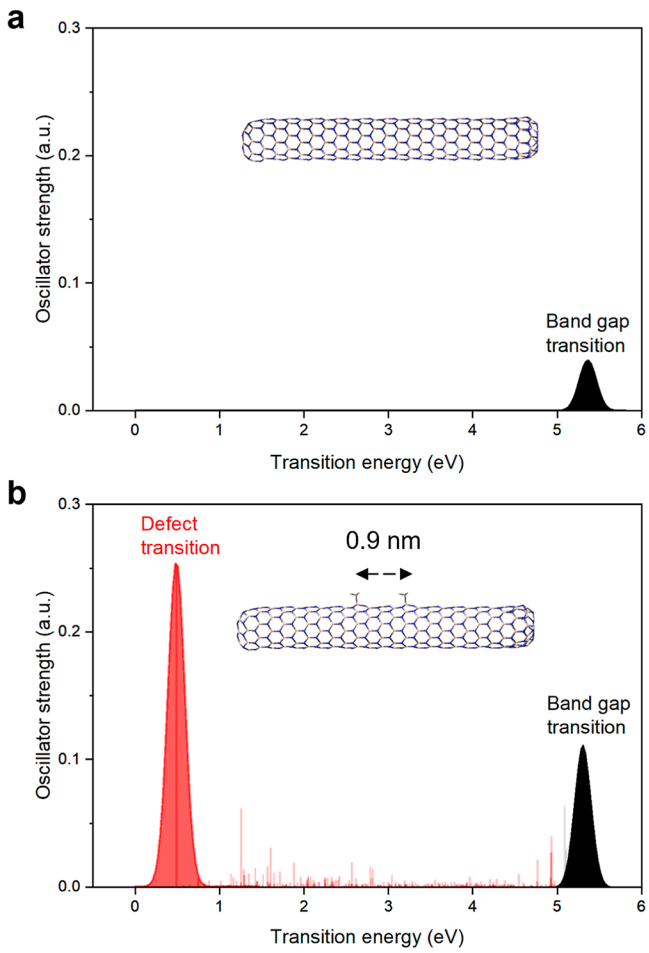

Figure 2. Large oscillator strength of the defect transition. (a) Oscillator strength of the pristine BNNT band gap transition. The strongest transition energy occurs around 5.6 eV with an oscillator strength of 0.039. (b) For the dimethyl f-BNNT (boron-site functionalized, ∼ 0.9 nm apart), the maximum oscillator strength (0.253) occurs at the minimum defect transition (0.4 eV, red curve) while the band gap transition is around 5.6 eV (black), consistent with the band gap transition energy of the pristine BNNT. The defect transition displays an oscillator strength 6.5 times as high as the pristine BNNT band gap transition. The defect (red curve) and band gap (black curve) transitions are shown with Gaussian functions (standard deviation: 0.1 eV).

suggested that the band gap transition energy of the (11,0) pristine carbon nanotube red shifts by ∼45 meV after incorporating sp^3 defects.[47]

We systematically altered the spacing between the boron-site methyl groups from 0.45 to 1.8 nm, in 0.45 nm increments corresponding to one unit cell length of the (9,0)-BNNT, as shown in Figure 3a. Since the defect orbitals are strongly localized around the boron-site bound to the methyl group (Figure 1), even at the largest defect spacing of 1.8 nm, we did not see any interaction between the defect orbitals and the ends of the BNNT (Figure S1). This variation in spacing allowed us to observe changes in the defect transition energy, which we plotted as a function of the methyl groups' distance in Figure 3b. Our findings reveal that, compared with the unmodified BNNT (Figure 3b, black square), the defect transition in the f-BNNTs significantly red shifts as the two defect sites were spaced further apart. This behavior aligns with what is observed in carbon nanotubes with sp^3 defects.[47] This

https://doi.org/10.1021/acs.jpcc.4c01586
J. Phys. Chem. C 2024, 128, 11672−11678

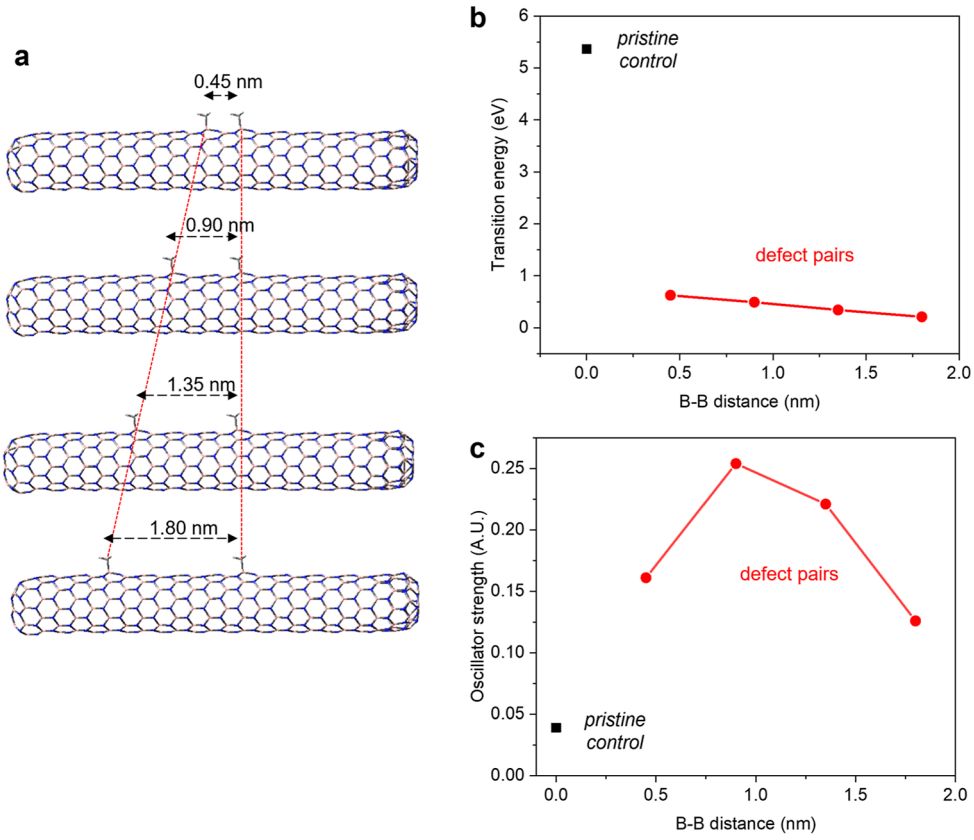

Figure 3. Distance-dependent defect coupling. (a) Molecular models of a 5 nm (9,0) f-BNNT with two methyl groups that are covalently bonded to boron atoms spaced 0.45 to 1.80 nm apart. (b) The lowest transition energy is a function of the distance between the two bonding boron sites (B−B distance) separated by 0.45, 0.9, 1.35, and 1.8 nm (red dots), while 0 nm represents a pristine BNNT (black dot). (c) Oscillator strength as a function of the distance between the two bonding boron sites (B−B distance). The oscillator strength of the defect transition peaks at 0.9 nm and then decreases (red dots). For comparison, the pristine BNNT control is also plotted (black dot).

result shows that the methyl pair defect transition in BNNTs is tunable in two distinct ways: first, introducing these defects alters the BNNT emission from the UV to the IR spectrum (from 5.4 to 0.63 eV); and second, the transition energy can be further tuned from the near-IR to mid-IR range (approximately 0.21−0.63 eV) by changing the distance between the functional groups (ranging from 0.45 to 1.8 nm).

Additionally, we calculated the oscillator strength as a function of the distance between the boron-site methyl groups, as shown in Figure 3c. The oscillator strength reached its peak value of 0.254 at a 0.9 nm distance between the groups and declined for larger separations, falling to 0.126 at a 1.8 nm distance. Importantly, the oscillator strength was found to be at least three times stronger than that of the pristine BNNT band gap transition (0.039) across all investigated distances between the functional groups. This enhancement highlights the significant impact of functional group spacing on the optical properties of BNNTs, offering a pathway to tailor these materials for specific applications by manipulating the distance between functional groups.

We note that traditional TD-DFT calculations using global hybrid functionals with a low exact exchange ratio may fail to capture long-range effects between the two functional groups. To assess the impact of these long-range effects, we additionally performed TD-DFT calculations using CAM-B3LYP, known for its long-range correction,[48] and compared its outcomes with those obtained from the global hybrid functionals. The CAM-B3LYP functional corrects the over-estimation by B3LYP on interaction energies, especially in cases where the basis sets of two interacting functional groups overlap. The result from the CAM-B3LYP functional shows a strong IR range defect transition compared with pristine band gap transition as predicted by the B3LYP functional. We also employed another long-range corrected functional, wB97XD, to corroborate our TD-DFT findings, and the result was consistent with the CAM-B3LYP results.[49] These enhanced calculations with long-range corrected functionals reaffirmed our conclusion that strong defect-induced transitions can occur within the IR spectral range in functionalized BNNTs (Figure S2).

Furthermore, we explored how the attachment of methyl group to nitrogen sites in f-BNNTs affects their optical properties. Our simulations revealed that such functionalization leads to a notable red shift in the minimum defect transition energy to the IR range (∼1 eV), with a marked increase in oscillator strength compared to the unmodified BNNT (Figure S3). The energy associated with these defect transitions can be similarly tuned by varying the distance between the two methyl groups, ranging from 0.45 to 1.8 nm. Increasing the spacing between the two methyl groups results in a reduction in the defect transition energy, as shown in Figure S3. The highest oscillator strength for the nitrogen-site f-BNNT (0.221) is predicted for the 1.35 nm spacing, which is slightly smaller than the 0.9 nm spaced boron-site f-BNNT (0.254). Notably, a minimal separation of 0.45 nm between the groups increases the defect transition energy to 3.2 eV, placing

https://doi.org/10.1021/acs.jpcc.4c01586
J. Phys. Chem. C 2024, 128, 11672−11678

it within the UV range. At this proximity, the electrons tend to localize at one of the two defect sites (Figure S4a). The localization is potentially due to symmetry breaking based on analysis of the bond angles, which significantly deviate from the ideal tetrahedral angle (109.5°), especially noticeable at the 0.45 nm separation (Figure S4b).

To compare the sp^3 defect transition to other known defects in BNNTs, we also investigated four vacancy and substitution defects, including a nitrogen vacancy adjacent to a nitrogen atom substituting a boron (V_NN_B), a nitrogen vacancy adjacent to a carbon atom substituting a boron (V_NC_B), a nitrogen vacancy (V_N), and a boron vacancy (V_B) in the BNNTs.[50] Figure 4 shows the oscillator strength of the lowest defect

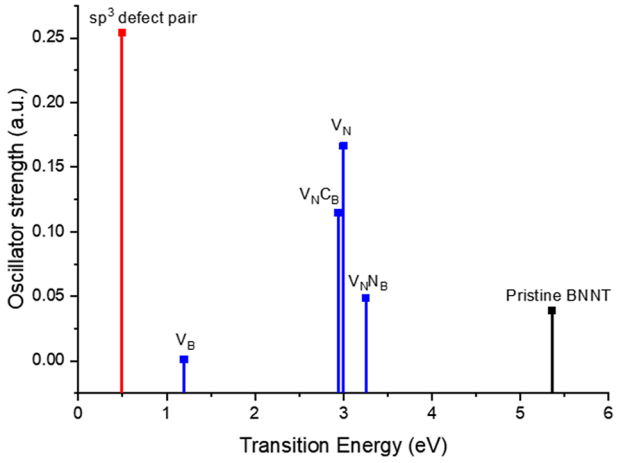

Figure 4. The dimethyl sp^3 defect pair exhibits stronger oscillator strength compared to the vacancy/substitution defects. The four different vacancy/substitution defects (V_B, V_NC_B, V_N, and V_NN_B) were modeled using the same 5 nm-long (9,0)-BNNT that was used to host the sp^3 defect pair (boron-site functionalized, 0.9 nm apart).

transitions of these vacancy/substitution defects. Among them, V_NC_B, V_N, and V_NN_B exhibit strong oscillator strength that is higher than the pristine BNNT, which we attribute to the strong overlap between the HOMO and LUMO (Figure S5). Among the four vacancy and substitution defects, V_N displays the highest oscillator strength of 0.1664. However, the transition is not as strong as that of dimethyl f-BNNTs. The highest oscillator strength of the boron-site f-BNNT (0.9 nm spacing) is 1.5 times higher (0.254) than V_N. Similarly, the highest oscillator strength of the f-BNNT functionalized at nitrogen sites (1.35 nm spacing) is 1.3-times higher (0.221) than V_N (Figure S2), suggesting the strong potential of sp^3 defects in BNNTs as bright quantum emitters.

The electronic structure of BNNTs is generally diameter independent.[2] As h-BN can be thought of as an infinite diameter BNNT, the bright IR-range defect transitions that occur in BNNTs should also occur in h-BN.[1] To investigate, we modeled an infinite sheet of pristine h-BN and functionalized h-BN (f-h-BN) using two-dimensional PBCs and compared the electronic structure to an infinitely long pristine (9,0)-BNNT and functionalized BNNT (f-BNNT) modeled using a one-dimensional PBC. For the f-h-BN and f-BNNT, a pair of methyl groups was covalently functionalized at boron sites spaced 0.9 nm apart. The supercell size of both f-h-BN and f-BNNT is 2.5 nm, and the size of the electron localization around the defect sites is ~0.9 nm (Figure S6). Since the size of the electron localization around the defect sites is smaller than the super cell size, the defect interaction mainly occurs within the super cell, not between neighboring cells. Compared to the h-BN model, the pristine BNNT generally has lower energy orbitals (Figure 5). However, the HOMO−LUMO

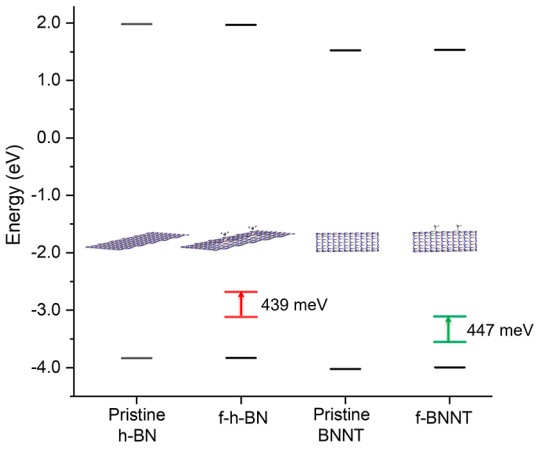

Figure 5. Energy diagrams of frontier molecular orbitals for pristine and dimethyl-functionalized models of h-BN and BNNT. Despite the difference in curvature, the h-BN sheet and BNNT are modified by the two methyl groups in a nearly identical manner, introducing within their band gap two new defect states with transition energies of 0.439 and 0.447 eV, respectively.

energy gap is roughly the same for the two systems (5.818 eV for h-BN vs 5.548 eV for BNNT), with the difference likely being due to curvature effects in the BNNT.[51] When we added the methyl pair defects to the systems, two new defect states appeared within the band gap for both f-BNNT and f-h-BN. Similar to the trend in the pristine models, the new defect orbitals are lower in energy for the f-BNNT model compared to f-h-BN, but the energy gap between the HOMO and LUMO is almost the same for the f-BNNT and f-h-BN (0.447 vs 0.439 eV). Moreover, the HOMO−LUMO overlap is more substantial in f-h-BN than in h-BN (Figure S6). This result suggests that a strong IR-range defect transition may occur in f-h-BN, as observed similarly for the f-BNNT.

The oscillator strength describes the likelihood of an electronic transition from the ground to an excited state, or vice versa, and high oscillator strength does not directly mean bright emission. Although further research is required, it is reasonable to argue that f-BNNT is potentially bright. First, based on Shiraki et al.'s observation,[41] hexyl-functionalized boron sites in f-BNNT emitted new photoluminescence at 334 and 413 nm. This corroborates that the emission from sp^3 defects in BNNT is not dark. Second, based on our calculation, V_NN_B defects (which are well studied as quantum emitters)[52,53] show smaller oscillator strength than sp^3 defect pairs. This suggests that sp^3 defects are brighter quantum light sources than V_NN_B defects, as long as there are no new nonradiative pathways introduced by the sp^3 defects.

CONCLUSIONS

DFT simulations of sp^3 defect pairs in BNNTs reveal a defect transition with an unexpectedly large oscillator strength occurring within the band gap. The sp^3 defects were modeled by covalently bonding two methyl groups to either B or N sites on model BNNTs. The defect transitions occur in the IR (0.21 to 0.63 eV), significantly red-shifted from the BNNT's band

https://doi.org/10.1021/acs.jpcc.4c01586
J. Phys. Chem. C 2024, 128, 11672−11678

gap transition (~5.6 eV). The oscillator strength of these defect transitions varies with the distance between the two methyl groups. Our simulations show that these sp^3 defects in BNNTs exhibit significantly high oscillator strength, by as much as 6.5 times compared to the pristine BNNT host, and surpassing that of vacancy/substitution defects. We attribute the high oscillator strength of these sp^3 defects to the small energy gap and high electron density overlap of the HOMO and LUMO states induced by the defect pair. Our calculations further suggest that these findings can be extended to h-BN. As a potential future research direction, different defect functional groups could be explored. The chemical nature of the sp^3 functional groups is known to have a notable effect on the emission properties in carbon nanotubes,[54] and we anticipate a similar type of functional tunability to be present with sp^3 defects in BNNTs. These results provide new insights into sp^3 defects in BNs and predict exciting prospects for exploiting quantum defects in boron nitride across various applications, including IR-range telecommunications and in situ biosensing.[9,12,13]

■ ASSOCIATED CONTENT

Supporting Information

The Supporting Information is available free of charge at https://pubs.acs.org/doi/10.1021/acs.jpcc.4c01586.

1.8 nm spaced f-BNNT electron density contour map, long-range corrected TD-DFT calculation, transition energy and oscillator strength of a nitrogen-site functionalized f-BNNT, electron density contour maps and center-to-vertex angles of an sp^3 defect site in the f-BNNT, electron density contour maps of the frontier orbitals of different vacancy/substitution defects in BNNTs, close-up images of the modeled vacancy/substitution defects, and electron density contour maps of the frontier orbitals of h-BN and f-h-BN (PDF)

■ AUTHOR INFORMATION

Corresponding Author

YuHuang Wang − *Department of Chemistry and Biochemistry, University of Maryland, College Park, Maryland 20770, United States; Chemical Physics Program and Maryland NanoCenter, University of Maryland, College Park, Maryland 20770, United States;* orcid.org/0000-0002-5664-1849; Email: yhw@umd.edu

Authors

Seungyeop Lee − *Department of Chemistry and Biochemistry, University of Maryland, College Park, Maryland 20770, United States;* orcid.org/0009-0009-1352-603X

Jacob Fortner − *Chemical Physics Program, University of Maryland, College Park, Maryland 20770, United States;* orcid.org/0000-0002-2379-0151

Complete contact information is available at: https://pubs.acs.org/10.1021/acs.jpcc.4c01586

Notes

The authors declare no competing financial interest.

■ ACKNOWLEDGMENTS

This work is not directly supported by a federal grant. However, we gratefully acknowledge personnel support provided in part by the National Science Foundation (grant no. CHE2204202) and the Center for Enhanced Nanofluidic Transport (CENT), an Energy Frontier Research Center funded by the U.S. Department of Energy, Office of Science, Basic Energy Sciences under award no. DE-SC0019112. We also gratefully acknowledge the University of Maryland supercomputing resources (http://hpcc.umd.edu) made available for conducting part of the quantum chemical calculations reported in this paper. The authors thank A. Brozena, J. Klos, B. Eller, D. Shin, and G. C. Schatz for valuable discussion.

■ REFERENCES

(1) Golberg, D.; Bando, Y.; Huang, Y.; Terao, T.; Mitome, M.; Tang, C. C.; Zhi, C. Y. Boron Nitride Nanotubes and Nanosheets. *ACS Nano* **2010**, *4* (6), 2979−2993.

(2) Jakubinek, M. B.; Kim, K. S.; Kim, M. J.; Marti, A. A.; Pasquali, M. Recent advances and perspective on boron nitride nanotubes: From synthesis to applications. *J. Mater. Res.* **2022**, *37* (24), 4403−4418.

(3) Haubner, R.; Wilhelm, M.; Weissenbacher, R.; Lux, B. Boron nitrides - Properties, synthesis and applications. *High Performance Non-Oxide Ceramics II*; Springer, 2002; Vol. *102*, pp 1−45.

(4) Rubio, A.; Corkill, J. L.; Cohen, M. L. THEORY OF GRAPHITIC BORON-NITRIDE NANOTUBES. *Phys. Rev. B* **1994**, *49* (7), 5081−5084.

(5) Li, F. F.; Lu, J. Z.; Tan, G. P.; Ma, M. M.; Wang, X. N.; Zhu, H. J. Boron nitride nanotubes composed of four- and eight-membered rings. *Phys. Lett. A* **2019**, *383* (1), 76−82.

(6) Nakanishi, R.; Kitaura, R.; Warner, J. H.; Yamamoto, Y.; Arai, S.; Miyata, Y.; Shinohara, H. Thin single-wall BN-nanotubes formed inside carbon nanotubes. *Sci. Rep.* **2013**, *3*, 1385.

(7) Ciofani, G.; Danti, S.; Genchi, G. G.; Mazzolai, B.; Mattoli, V. Boron Nitride Nanotubes: Biocompatibility and Potential Spill-Over in Nanomedicine. *Small* **2013**, *9* (9−10), 1672−1685.

(8) Merlo, A.; Mokkapati, V.; Pandit, S.; Mijakovic, I. Boron nitride nanomaterials: biocompatibility and bio-applications. *Biomater. Sci.* **2018**, *6* (9), 2298−2311.

(9) Chen, X.; Wu, P.; Rousseas, M.; Okawa, D.; Gartner, Z.; Zettl, A.; Bertozzi, C. R. Boron Nitride Nanotubes Are Noncytotoxic and Can Be Functionalized for Interaction with Proteins and Cells. *J. Am. Chem. Soc.* **2009**, *131* (3), 890−891.

(10) Setlow, R. B. Cyclobutane-type pyrimidine dimers in polynucleotides. *Science* **1966**, *153* (3734), 379−386.

(11) Li, C. Y.; Wang, Q. B. Challenges and Opportunities for Intravital Near-Infrared Fluorescence Imaging Technology in the Second Transparency Window. *ACS Nano* **2018**, *12* (10), 9654−9659.

(12) Flannigan, L.; Yoell, L.; Xu, C. Q. Mid-wave and long-wave infrared transmitters and detectors for optical satellite communications-a review. *J. Opt.* **2022**, *24* (4), 043002−043041.

(13) Cao, X.; Zopf, M.; Ding, F. Telecom wavelength single photon sources. *J. Semicond.* **2019**, *40* (7), 071901−071911.

(14) Luo, X. W.; Zhang, C. W.; Novikova, I.; Qian, C.; Du, S. W. Wavelength conversion for single-photon polarization qubits through continuous-variable quantum teleportation. *Phys. Rev. A* **2022**, *105* (5), 052444−052447.

(15) Aharonovich, I.; Neu, E. Diamond Nanophotonics. *Adv. Opt. Mater.* **2014**, *2* (10), 911−928.

(16) Lesik, M.; Tetienne, J. P.; Tallaire, A.; Achard, J.; Mille, V.; Gicquel, A.; Roch, J. F.; Jacques, V. Perfect preferential orientation of nitrogen-vacancy defects in a synthetic diamond sample. *Appl. Phys. Lett.* **2014**, *104* (11), 1−5.

(17) He, Y. M.; Clark, G.; Schaibley, J. R.; He, Y.; Chen, M. C.; Wei, Y. J.; Ding, X.; Zhang, Q.; Yao, W.; Xu, X. D.; Lu, C. Y.; Pan, J. W. Single quantum emitters in monolayer semiconductors. *Nat. Nanotechnol.* **2015**, *10* (6), 497−502.

(18) Piao, Y. M.; Meany, B.; Powell, L. R.; Valley, N.; Kwon, H.; Schatz, G. C.; Wang, Y. H. Brightening of carbon nanotube

photoluminescence through the incorporation of sp(3) defects. *Nat. Chem.* **2013**, *5* (10), 840−845.
(19) He, X. W.; Hartmann, N. F.; Ma, X. D.; Kim, Y.; Ihly, R.; Blackburn, J. L.; Gao, W. L.; Kono, J.; Yomogida, Y.; Hirano, A.; et al. Tunable room-temperature single-photon emission at telecom wavelengths from *sp* 3 defects in carbon nanotubes. *Nat. Photonics* **2017**, *11* (9), 577−582.
(20) Grosso, G.; Moon, H.; Lienhard, B.; Ali, S.; Efetov, D. K.; Furchi, M. M.; Jarillo-Herrero, P.; Ford, M. J.; Aharonovich, I.; Englund, D. Tunable and high-purity room temperature single-photon emission from atomic defects in hexagonal boron nitride. *Nat. Commun.* **2017**, *8*, 705−708.
(21) Mendelson, N.; Chugh, D.; Reimers, J. R.; Cheng, T. S.; Gottscholl, A.; Long, H.; Mellor, C. J.; Zettl, A.; Dyakonov, V.; Beton, P. H.; et al. Identifying carbon as the source of visible single-photon emission from hexagonal boron nitride. *Nat. Mater.* **2021**, *20* (3), 321−328.
(22) Tran, T. T.; Bray, K.; Ford, M. J.; Toth, M.; Aharonovich, I. Quantum emission from hexagonal boron nitride monolayers. *Nat. Nanotechnol.* **2016**, *11* (1), 37−41.
(23) Kurtsiefer, C.; Mayer, S.; Zarda, P.; Weinfurter, H. Stable solid-state source of single photons. *Phys. Rev. Lett.* **2000**, *85* (2), 290−293.
(24) Michl, J.; Teraji, T.; Zaiser, S.; Jakobi, I.; Waldherr, G.; Dolde, F.; Neumann, P.; Doherty, M. W.; Manson, N. B.; Isoya, J.; et al. Perfect alignment and preferential orientation of nitrogen-vacancy centers during chemical vapor deposition diamond growth on (111) surfaces. *Appl. Phys. Lett.* **2014**, *104* (10), 1−5.
(25) Kok, P.; Munro, W. J.; Nemoto, K.; Ralph, T. C.; Dowling, J. P.; Milburn, G. J. Linear optical quantum computing with photonic qubits. *Rev. Mod. Phys.* **2007**, *79* (1), 135−174.
(26) Aspuru-Guzik, A.; Walther, P. Photonic quantum simulators. *Nat. Phys.* **2012**, *8* (4), 285−291.
(27) Giovannetti, V.; Lloyd, S.; Maccone, L. Advances in quantum metrology. *Nat. Photonics* **2011**, *5* (4), 222−229.
(28) Lo, H. K.; Curty, M.; Tamaki, K. Secure quantum key distribution. *Nat. Photonics* **2014**, *8* (8), 595−604.
(29) Scarani, V.; Bechmann-Pasquinucci, H.; Cerf, N. J.; Dusek, M.; Lutkenhaus, N.; Peev, M. The security of practical quantum key distribution. *Rev. Mod. Phys.* **2009**, *81* (3), 1301−1350.
(30) Kwon, H.; Furmanchuk, M.; Kim, M.; Meany, B.; Guo, Y.; Schatz, G. C.; Wang, Y. H. Molecularly Tunable Fluorescent Quantum Defects. *J. Am. Chem. Soc.* **2016**, *138* (21), 6878−6885.
(31) Kwon, H.; Kim, M.; Meany, B.; Piao, Y. M.; Powell, L. R.; Wang, Y. H. Optical Probing of Local pH and Temperature in Complex Fluids with Covalently Functionalized, Semiconducting Carbon Nanotubes. *J. Phys. Chem. C* **2015**, *119* (7), 3733−3739.
(32) Wang, P.; Fortner, J.; Luo, H. B.; Kaos, J.; Wu, X. J.; Qu, H. R.; Chen, F.; Li, Y.; Wang, Y. H. Quantum Defects: What Pairs with the Aryl Group When Bonding to the sp(2) Carbon Lattice of Single-Wall Carbon Nanotubes? *J. Am. Chem. Soc.* **2022**, *144* (29), 13234−13241.
(33) He, X.; Htoon, H.; Doorn, S. K.; Pernice, W. H. P.; Pyatkov, F.; Krupke, R.; Jeantet, A.; Chassagneux, Y.; Voisin, C. Carbon nanotubes as emerging quantum-light sources. *Nat. Mater.* **2018**, *17* (8), 663−670.
(34) Mandal, A. K.; Wu, X. J.; Ferreira, J. S.; Kim, M.; Powell, L. R.; Kwon, H.; Groc, L.; Wang, Y. H.; Cognet, L. Fluorescent sp(3) Defect-Tailored Carbon Nanotubes Enable NIR-II Single Particle Imaging in Live Brain Slices at Ultra-Low Excitation Doses. *Sci. Rep.* **2020**, *10* (1), 5286−5289.
(35) Kim, M.; Chen, C.; Yaari, Z.; Frederiksen, R.; Randall, E.; Wollowitz, J.; Cupo, C.; Wu, X. J.; Shah, J.; Worroll, D.; et al. Nanosensor-based monitoring of autophagy-associated lysosomal acidification in vivo. *Nat. Chem. Biol.* **2023**, *19*, 1448−1457.
(36) Qu, H. R.; Wu, X. J.; Fortner, J.; Kim, M.; Wang, P.; Wang, Y. H. Reconfiguring Organic Color Centers on the sp(2) Carbon Lattice of Single-Walled Carbon Nanotubes. *ACS Nano* **2022**, *16* (2), 2077−2087.
(37) Kwon, H.; Kim, M.; Nutz, M.; Hartmann, N. F.; Perrin, V.; Meany, B.; Hofmann, M. S.; Clark, C. W.; Htoon, H.; Doorn, S. K.; Hoegele, A.; Wang, Y. H. Probing Trions at Chemically Tailored Trapping Defects. *ACS Cent. Sci.* **2019**, *5* (11), 1786−1794.
(38) Hu, W.; Cao, X. R.; Zhang, Y. J.; Li, T. D.; Jiang, J.; Luo, Y. Tunable Single-Photon Emission by Defective Boron-Nitride Nanotubes for High-Precision Force Detection. *J. Phys. Chem. C* **2019**, *123* (14), 9624−9628.
(39) Attaccalite, C.; Wirtz, L.; Marini, A.; Rubio, A. Efficient Gate-tunable light-emitting device made of defective boron nitride nanotubes: from ultraviolet to the visible. *Sci. Rep.* **2013**, *3*, 2698−2707.
(40) Azevedo, S.; Kaschny, J. R.; de Castilho, C. M. C.; Mota, F. D. Electronic structure of defects in a boron nitride monolayer. *Eur. Phys. J. B* **2009**, *67* (4), 507−512.
(41) Shiraki, T.; Saito, R.; Saeki, H.; Tanaka, N.; Harano, K.; Fujigaya, T. Defect Photoluminescence from Alkylated Boron Nitride Nanotubes. *Chem. Lett.* **2023**, *52* (1), 44−47.
(42) Melchor, S.; Dobado, J. A. CoNTub: An algorithm for connecting two arbitrary carbon nanotubes. *J. Chem. Inf. Comput. Sci.* **2004**, *44* (5), 1639−1646.
(43) Hanwell, M. D.; Curtis, D. E.; Lonie, D. C.; Vandermeersch, T.; Zurek, E.; Hutchison, G. R. Avogadro: an advanced semantic chemical editor, visualization, and analysis platform. *J. Cheminf.* **2012**, *4*, 17.
(44) Lin, C. D.; Tang, P. Kekule count in capped zigzag boron-nitride nanotubes. *J. Chem. Inf. Comput. Sci.* **2004**, *44* (1), 13−20.
(45) Braslavsky, S. E. Glossary of terms used in Photochemistry 3rd Edition (IUPAC Recommendations 2006). *Pure Appl. Chem.* **2007**, *79* (3), 293−465.
(46) Hilborn, R. C. Einstein coefficients, cross sections, f values, dipole moments, and all that. *Am. J. Phys.* **1982**, *50* (11), 982−986.
(47) Fortner, J.; Wang, Y. H. Quantum Coupling of Two Atomic Defects in a Carbon Nanotube Semiconductor. *J. Phys. Chem. Lett.* **2022**, *13* (38), 8908−8913.
(48) Yanai, T.; Tew, D. P.; Handy, N. C. A new hybrid exchange-correlation functional using the Coulomb-attenuating method (CAM-B3LYP). *Chem. Phys. Lett.* **2004**, *393* (1−3), 51−57.
(49) Chai, J. D.; Head-Gordon, M. Long-range corrected hybrid density functionals with damped atom-atom dispersion corrections. *Phys. Chem. Chem. Phys.* **2008**, *10* (44), 6615−6620.
(50) Abdi, M.; Chou, J. P.; Gali, A.; Plenio, M. B. Color Centers in Hexagonal Boron Nitride Monolayers: A Group Theory and Ab Initio Analysis. *ACS Photonics* **2018**, *5* (5), 1967−1976.
(51) Ortix, C.; van den Brink, J. Effect of curvature on the electronic structure and bound-state formation in rolled-up nanotubes. *Phys. Rev. B* **2010**, *81* (16), 165419−165425.
(52) Tran, T. T.; Bray, K.; Ford, M. J.; Toth, M.; Aharonovich, I. Quantum emission from hexagonal boron nitride monolayers. *Nat. Nanotechnol.* **2016**, *11* (1), 37−41.
(53) Grosso, G.; Moon, H.; Lienhard, B.; Ali, S.; Efetov, D. K.; Furchi, M. M.; Jarillo-Herrero, P.; Ford, M. J.; Aharonovich, I.; Englund, D. Tunable and high-purity room temperature single-photon emission from atomic defects in hexagonal boron nitride. *Nat. Commun.* **2017**, *8*, 705.
(54) Brozena, A. H.; Kim, M.; Powell, L. R.; Wang, Y. Controlling the optical properties of carbon nanotubes with organic colour-centre quantum defects. *Nat. Rev. Chem* **2019**, *3* (6), 375−392.

https://doi.org/10.1021/acs.jpcc.4c01586
J. Phys. Chem. C 2024, 128, 11672−11678